JOURNAL OF PROPULSION AND POWER
Vol. 14, No. 3, May–June 1998

Temperature and Species Measurements in a Low-Thrust Hydrogen/Oxygen Rocket Engine

Wilhelmus A. de Groot*
NYMA, Inc., Brook Park, Ohio 44142

Raman scattering measurements are obtained inside the combustion chamber and near the nozzle exit plane of two experimental models of an onboard hydrogen/oxygen thruster. Temperature, oxygen number density, and water number density data are obtained in the combustion chamber at the injector exit of one thruster. These data show incomplete combustion in the injector section prior to injection of film cooling, and strongly stratified injector temperature and species profiles. Using the measured injector data as input to an axisymmetric Navier–Stokes code does not improve global performance parameter predictions over predictions using fully uniform injector exit profiles. In both cases, performance is underpredicted. Additionally, temperature and oxygen number density data are obtained at the exit plane of the low-area-ratio-nozzle of the second thruster with the same injector installed. A comparison of these measured data with analytical predictions that utilize two different sets of input conditions show significant discrepancies for both cases. The laminar nature of the flow, which the axisymmetric code predicts will occur, precludes sufficient mixing to increase global performance predictions. Three-dimensional modeling of both the injector section and the combustion chamber is needed to obtain more accurate global performance predictions for this thruster.

Introduction

THE cost-effectiveness of current satellites can be improved by increasing the payload at the expense of onboard propellant mass. This requires, to retain the same mission capabilities, that onboard propulsion systems need to perform more efficiently. Several methods are being pursued that have the potential to accomplish this; namely, the development of high-temperature, oxidation-resistant materials that allow higher combustion temperatures without the need for inefficient wall film cooling,[1–3] a refined component design that leads to better mixing and more uniform flow properties,[4] and innovative propellant combinations that provide a higher I_{sp} than current flight systems.[5] Additionally, the utilization of more benign propellant combinations will enhance safety, facilitate environmental compliance, and improve cost-effectiveness by reducing propellant loading and handling.

The JANNAF–TDK methodology and computational fluid dynamics (CFD) codes are used to evaluate rockets that are under development and to establish the effect of design changes on existing rockets. For high- and medium-thrust rockets, an acceptable prediction of the global performance parameters, such as thrust and I_{sp}, can be made with the current level of predictive technology. Using these codes to predict the performance and thermal behavior of certain low-thrust rockets, however, leads to inaccurate results, the specific causes of which are not yet identified. Richter and Price,[6] for example, use a standard JANNAF ODE method to predict the I_{sp} of a 220 N gaseous hydrogen/oxygen (GH_2/GO_2) thruster operating at various stoichiometries. They show an overprediction of 12.2% at an oxygen-to-fuel (O/F) mole ratio of 4 (I_{sp} of 423 vs 376 s), and 18.2% at an O/F ratio of 7 (I_{sp} of 399 vs 338 s). Weiss[7] uses the Navier–Stokes-based axisymmetric RPLUS code, including a k-ε turbulence model, to predict performance parameters of two 110 N thrusters. Predicted values for one thruster, operating at an overall O/F ratio of 6.8 with a fuel–film cooling (FFC) percentage of 15%, are higher by 23% in thrust (137 vs 111 N) and 18% in I_{sp} (404 vs 348 s) than the measured values. Predicted values for the second thruster, operating at an overall O/F ratio of 6.7 and a FFC percentage of 61% are approximately 4 and 3% lower than the measured values (thrust of 110 vs 114 N; I_{sp} of 342 vs 351). Improved predictions for these rockets must be based on a better understanding of the physics of small rockets, a refined analysis of the individual rocket, and an increase in numerical capabilities. Such developments will be greatly aided by the calibration of CFD codes using measured, localized, fluid dynamic, and thermodynamic data.

Onboard rockets are set apart from the total family of rockets by their small size. This and the associated three-dimensional nature of the flow results in strong temperature, species, and velocity gradients, which often cannot be approximated with conventional codes. The comparison of measured and predicted global parameters are not a good indicator of how well CFD codes perform for predicting low-thrust rocket performance. To improve upon sections of the codes that use empirical relations (which are no longer adequate for these extreme gradient flowfields), a much more rigorous test would be an acceptable comparison between predicted local flowfield data with local data obtained from experiments. Historically, because of the inaccessibility of the rocket core and the hostile nature of the reacting flow, such measured local data were hard to obtain. The availability of recently developed nonintrusive techniques based on laser light scattering from molecules, such as Rayleigh and Raman scattering, enabled a number of these desired parameters to be quantified. Initial measurements were obtained in the easily accessible nozzle exit plane. Rayleigh scattering provided velocity, translational temperature, and some species density data.[8,9] Raman scattering provided vibrational temperature and major species density data.[10] Comparison of both these sets of measured data with results from CFD codes, such as the Navier–Stokes-based RPLUS code[11,12] and the JANNAF TDK/VIPER/SPF[13] methodology, indicated that an accurate prediction could only be made if detailed, accurate boundary conditions were available.

The axisymmetric RPLUS code consistently underpredicted the global performance parameters (I_{sp} and thrust) of the

Received Jan. 2, 1996; revision received June 17, 1997; accepted for publication Nov. 10, 1997.

*Senior Research Engineer, Aerospace Technology Department. Senior Member AIAA.

thruster under investigation. This underprediction was surprising because the upstream boundary conditions assumed fully reacted injector flow. The basic calculations showed that approximately 20% of the fuel–film was consumed by the core. The global parameters could be predicted accurately if an additional 10% of the hydrogen fuel–film at the wall would be consumed by the core. This was achieved by artificially increasing the diffusivity. But because the code predicted the combustion chamber flow to be fully laminar, with a boundary-layer Reynolds number of 1×10^4 and a core Reynolds number of 6×10^4, no additional mixing mechanism was present to affect this increased core–film mixing. The growth of the shear layer between the core flow and the fuel–film, which could have contributed to such mixing, was suppressed by the presence of the wall.

Because accurate injector mixing data were absent, injector exit profiles were assumed in the modeling efforts. Errors made in these assumptions tended to propagate downstream from the injector, through the combustor, throat section, nozzle, and plume. For rigorous modeling, a detailed injector profiling was necessary. Thus, a two-dimensional, optically accessible chamber was built in which injector species and temperature profiles could be measured at the injector exit plane. This paper presents these measurements and the measurements taken in the nozzle exit plane, and compares the nozzle exit results with predictions made using assumed injector profiles and the measured profiles.

Experiment

The rocket under investigation is a 110 N, regenerative, and film-cooled GH_2/GO_2 thruster originally designed for the space station.[14] A simplified schematic of the flowfield is shown in Fig. 1. Oxygen is injected at the head end of the injector, near the base of the spark plug. The hydrogen flows through small cooling passages inside the nozzle/chamber walls to cool the thruster. In addition, a fuel–film is used to keep the wall temperature below material limits and as a barrier to protect the wall against oxidation. At the head end of the thruster, the fuel flow is divided by a splitter plate against the platelet stack. Varying splitter plates allow varying fuel–film percentages. The percentage of fuel needed to film cool this design is between 60 and 75%. The remainder of the fuel is radially injected, through 12 equal-angle-spaced ports of a platelet injector, into the core region of pure oxygen near the spark plug tip. During ignition, a spark plug in the center excites the oxygen, which then reacts with the hydrogen. After ignition, combustion is sustained in the bluff-body recirculation region behind the spark plug tip, where velocities are relatively low and good (turbulent) mixing takes place. This primary combustion zone causes an oxygen-rich product mixture to emerge from the primary combustion region. For convenience, this primary region is referred to in this paper as injector (Fig. 1). The injector sleeve between the fuel–film and this oxygen-rich core generates a secondary combustion shear layer where the fuel and oxygen mix and react. To achieve full wall protection, the film should be sufficiently thick to maintain wall coverage through the throat.

All thruster models are tested in a high-altitude simulation facility. A horizontal thrust stand holds the thrusters and measures the thrust. Together with the measured propellant mass flow rates and chamber pressure, these parameters enable the calculation of experimental I_{sp} and characteristic velocity C^* for a given thruster.

Initially, a full-scale engineering model with nozzle area ratio of 30:1 was tested for global parameter measurements and nozzle exit/plume measurements by means of Rayleigh scattering.[8,9] Two additional pieces of hardware were designed and manufactured that allowed optical access for number density and temperature measurements. For clarity, the characteristics of all three hardware items are summarized in Table 1. A two-dimensional, optically accessible thruster was fabricated to allow measurements to be taken on the composition of the flow emerging from the injector. Figures 2a and 2b show the schematic and the hardware, respectively. The purpose was to study the effect of the injector characteristics on the thruster performance and the accuracy of CFD predictions. This two-dimensional thruster accommodated the same injector as the low-area-ratio-thruster. The fuel–film sleeve insert, however, transitioned from a circular splitter plate into a rectangular sleeve section. The intent was to create a two-dimensional combustor flow. The effect of this sudden transition on the mixing and combustion in the injector section is not known, but is assumed to be limited to the corner areas of the square fuel–film sleeve. The fuel–film sleeve was designed with passages on the top and bottom of the injector, such that only the top and bottom plates had FFC. Both plates were water cooled in addition to the fuel–film cooling.

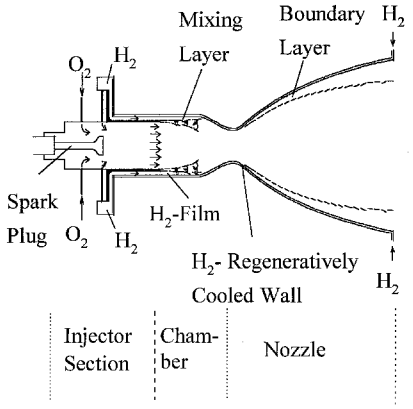

Fig. 1 Regeneratively cooled GH_2/GO_2 thruster flowfield schematic.

Optical access was provided through 12.5-mm-thick quartz windows in the side walls. These windows were protected from the high-temperature core flow by a nitrogen shroud injected through passages built into the head end of the thruster. The nitrogen film flow rate was approximately 36% of the total mass flow rate (0.019 kg/s N_2 vs 0.033 kg/s H_2 and O_2). The nitrogen shroud was expected to have some effect on the flow characteristics at the exit of the injector sleeve. Raman measurements at the injector exit plane, however, did not show the presence of nitrogen. And because nitrogen injection occurred downstream of the measurement points, the effect of the nitrogen cooling on the core flow at the measurement location was assumed to be negligible. The throat height and exit height were selected for geometric similarity with the axisymmetric rocket nozzle diameter and do not match the regenerative nozzle area ratio.

Operating conditions for this two-dimensional thruster were different than for the regeneratively cooled thruster because of a mismatch in the cross-sectional area of the throat and fuel–film passages and because of the dilution/cooling of the windows with nitrogen. The total propellant mass flow rate was 0.0332 kg/s. An overall O/F ratio of 6.0 was maintained during the experiments. Platelets split the hydrogen flow in two, using 55% of the fuel to film cool the walls and the remainder creating an injector O/F ratio of 13.3. The chamber pressure was 0.3 MPa (vs 0.5 MPa for the regeneratively cooled engines). Hydrogen accumulation in the altitude chamber limited test times with this model to 15 s.

An axisymmetric model was built with injector, chamber, and throat dimensions equal to the regenerative thruster, but with an area ratio of 1.86:1. A schematic of this model is shown in Fig. 3a and a photograph of the hardware in Fig. 3b. The area ratio was chosen based on a simple two-dimensional analysis that showed that the pressure at the exit plane was approximately 0.1 MPa. Calibration measurements indicated that at this pressure level, the major species number densities

Table 1 Characteristic data for three different test hardware items

Quantity	Engineering model thruster	Two-dimensional diagnostics thruster	Low-area-ratio thruster
Figure no.	1	2	3
Oxygen mass flow, kg/s	0.0278	0.0284	0.0278
Hydrogen mass flow, kg/s	0.0054	0.0047	0.0054
Nitrogen coolant flow, kg/s	N/A	0.019	N/A
Overall O/F ratio	5.13	6.0	5.13
Core O/F ratio	20.0	13.3	20.0
(FFC), %	75	55	75
Chamber pressure, MPa	0.5	0.3	0.5
Area ratio	30	7.65	1.86
Measured thrust, N	114	N/A	N/A
Cooling type	Hydrogen regenerative/ fuel–film	Hydrogen fuel–film; nitrogen shroud; water cooling	Hydrogen fuel–film; water cooling

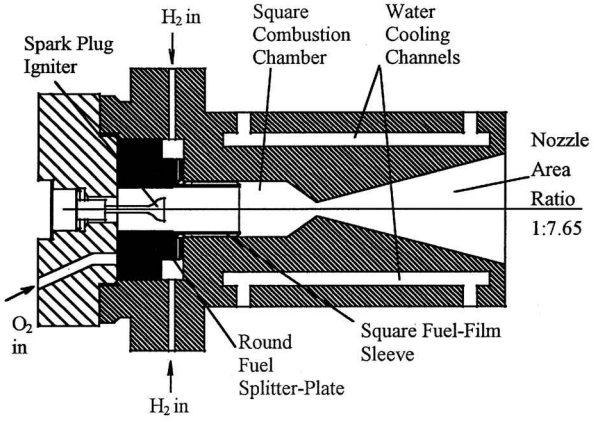

a)

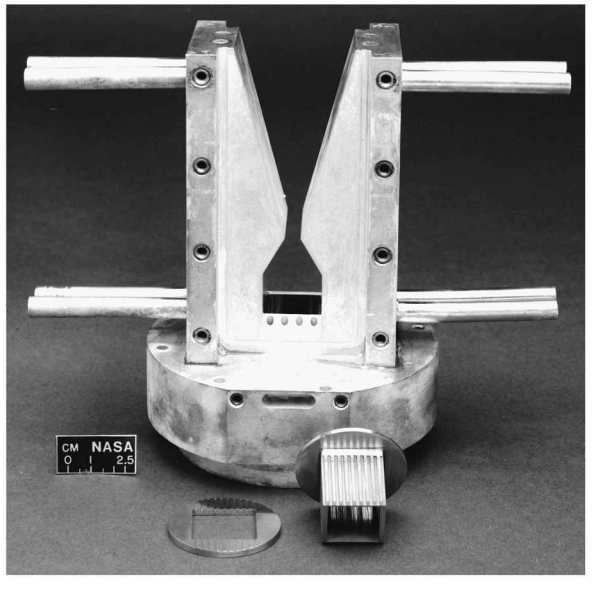

b)

Fig. 2 Two-dimensional diagnostics rocket: a) schematic and b) hardware.

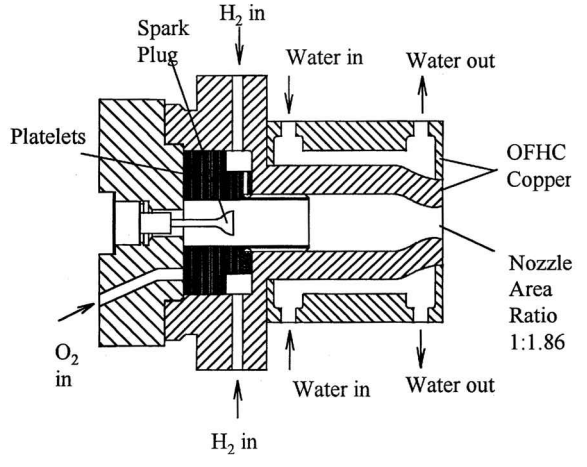

a)

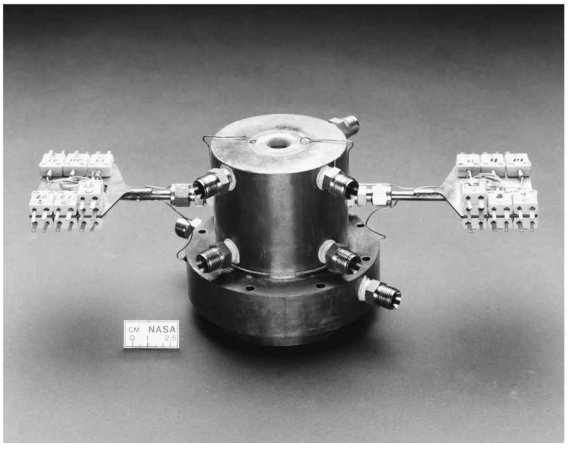

b)

Fig. 3 Low-area-ratio-nozzle rocket: a) schematic and b) hardware.

were sufficient for acceptable Raman measurements with the laboratory Raman measurement system. For simplicity, the model was designed with water instead of regenerative cooling of the chamber. This caused the injected hydrogen to be significantly cooler and the thruster to have lower performance as a result of the heat loss to the wall (in addition to the loss incurred as the result of the low-area-ratio-nozzle). It also required an adjustment in the CFD prediction because of a change in injection velocity and temperature of the hydrogen. Thermocouples that were recessed 0.16 cm away from the inner wall monitored wall temperatures throughout the thruster.

Operating conditions for this water-cooled chamber were comparable to the regenerative thruster. The same mass flow rate of 0.0332 kg/s gave a chamber pressure 0.5 MPa. The overall O/F ratio was 5.13 with an FFC of 75%, and an injector O/F ratio of 20. The fuel-injection temperature was lower (298 K) than for the regenerative thruster because of the absence of regenerative cooling. As the result of better diffuser performance with this thruster installed, test durations of 30 s were

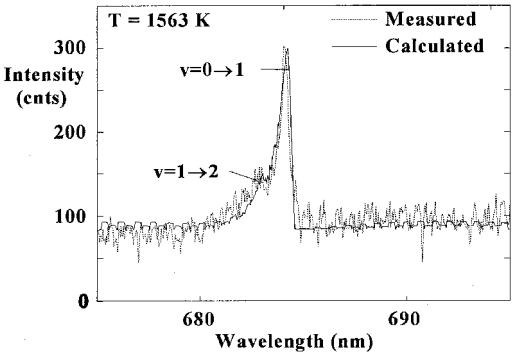

Fig. 4 Measured and calculated Raman Q-branch spectra of nitrogen.

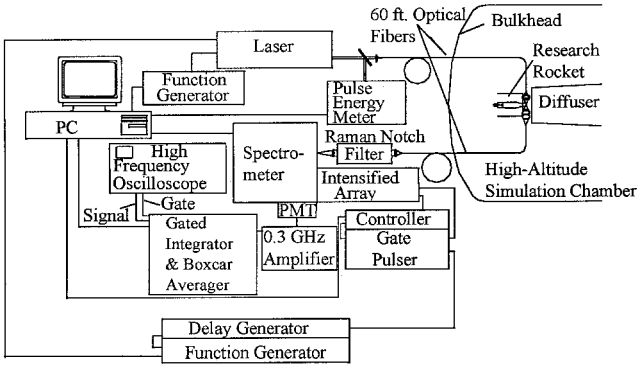

Fig. 5 Raman data acquisition schematic.

possible. No evidence of water condensation inside the thruster was found.

Measurement Approach

For nonintrusive measurements, spontaneous Raman scattering was chosen over methods that would provide stronger signal-to-noise ratios (SNR), such as coherent anti-Stokes Raman scattering (CARS), because of restrictions imposed by the geometry and the environment inside the high-altitude simulation facility. Furthermore, spontaneous Raman scattering was amenable to implementation in an optical fiber configuration. This was an important condition to gain access to the thruster installed inside the high-altitude simulation facility and to satisfy laboratory safety rules. Temperature and number densities of individual polyatomic species within a gas mixture can be extracted simultaneously. Excellent spatial and temporal resolution can be obtained with a judicious design of the optics and data acquisition system. The nonintrusive nature of the technique allows measurements in hostile environments without disturbing the flow character. The weakness of the scattering signal, however, virtually prohibits the application in luminous environments and typically allows only major species to be measured accurately. In the thruster experiments described in this paper, with gaseous hydrogen and gaseous oxygen as propellants, luminosity was low, creating an ideal environment for the application of spontaneous Raman scattering.

The Raman measurement uses the spectral content of light scattered when a mixture of molecules is exposed to incident, monochromatic light, such as laser light. The molecules exchange energy with the incident field during the scattering process. The fraction of the light scattered with the same frequency as the incident light is referred to as Rayleigh scattering and is not species specific. A fraction of the light is scattered with a frequency that is a combination of the incident frequency and quantized molecular rotational–vibrational frequencies. Depending on whether the molecule has lost energy or gained energy from the interaction with the scattered light quantum, these light fractions are called anti-Stokes and Stokes scattering, respectively. This part of the scattered light is species specific and is used to identify molecules, and measure their quantities and temperatures.

For gaseous GH_2/GO_2 thrusters, the species detected and analyzed are hydrogen, oxygen, and water. Other combustion intermediates and products will not appear long enough or in sufficient quantity to be detected. Spectral modeling of species focused on the previously listed species as well as on nitrogen which, because of its presence in air, is an excellent calibration gas.

A spectral simulation code coupled with a numerical curve-fitting routine was written for the diatomic species and water. The code included the effect of light polarization and geometrical configuration of the optics on the individually detected line strengths, which is more general than the conventionally used Raman scattering cross section. A generic approach to such calculations for diatomic molecules is given by James and Klemperer.[15] An excellent derivation for hydrogen is given by Shirley.[16] The molecular constants necessary to complete the equations for nitrogen, oxygen, and hydrogen can be found in Refs. 17–19. Temperature and number densities can be extracted by performing a Levenburg–Marquardt best-fit analysis of the measured spectra with computational spectra. An example best-fit from a spectrum obtained in the flame of a propane torch in quiescent air is shown in Fig 4. The first hot band ($v = 1 \rightarrow 2$) is clearly visible. The Raman measured temperature of 1563 K compared well with a corrected thermocouple measurement of 1498 K.

During all measurements it was assumed that instantaneous rotational and vibrational equilibration occurred. This allowed a single temperature to be inserted in the curvefit instead of separate rotational and vibrational temperatures. Separate measurements of rotational and vibrational temperatures on the thruster centerline from the combustor, through the throat and part of the nozzle, showed the assumption to be justified.[20,21]

A schematic of the experimental setup is shown in Fig. 5. A flashlamp-pumped dye laser generated a wavelength of approximately 597 nm using Rhodamine 590 (R6G) tuned to the strongest emission. This long wavelength assured that all spontaneous Raman emission occurred in a spectral area where fluorescence was virtually absent. Such fluorescence would make any Raman scattering undetectable because its emitted intensity is many orders of magnitude stronger (approximately 10^6–10^9 times).[22] With the selection of the tuning optics, the laser beam was optimized to a pulse energy of about 1.2 J/pulse with a full width at half-maximum (FWHM) bandwidth of 0.03 nm (0.8 cm^{-1}). The total pulse length was 2.2 μs. This long pulse length assured a low peak laser intensity, facilitating optical fiber transmission. It also precluded intrusive effects to the gas such as gas breakdown or ionization, and nonlinear processes such as stimulated Raman scattering. The long pulse length could have resulted in some sacrifice in temporal resolution. But because the characteristic time scales inside the thruster were relatively long ($\sim$100 μs), this was not expected to be a problem.

The temporal decay of the laser pulse energy was measured at the laser exit and then accounted for in the data reduction. The laser pulse was coupled by means of a microscope objective into an 800-μm optical fiber with metal jacket. The fiber guided the laser pulses through the blast wall that separated the clean room from the test facility and through the bulkhead of the high-altitude simulation chamber. In the chamber, the pulses were collimated and then refocused. Collection optics were positioned 90 deg from the focusing optics for the collection of Raman scattered light. This geometry reduced the chance of collecting stray laser light. The confluence of delivery and collection optics created a probe volume of about 0.7 mm^3. Baffles were placed in the delivery and collection optics and a beam stop was positioned to capture the laser pulses

(possible in the exit plane, not in the combustion chamber). This caused an additional reduction in interference of stray laser light.

The collection optics imaged the probe volume into a 800-μm optical fiber. This fiber guided the scattered light back through the bulkhead and through the wall of the clean room. There the light was collimated and passed through a Raman notch filter, an optical filter with attenuation at the laser line of 10^{-6}, with transmission at the Raman lines of more than 90%. A lens was used to refocus the light into a 0.5-m spectrometer with a 1200-groove/mm grating. This gave a spectral dispersion of 1.6 nm/mm.

Two strategies were followed for processing the signal. As a result of low number densities in the low-area-ratio nozzle, a gallium-arsenide photomultiplier tube (PMT) was used because of its high gain relative to linear arrays. The PMT signal was amplified and processed in a boxcar averager and integrator. There, the scattering signal was gated and measured over the duration of the laser pulse. Each pulse was corrected for laser pulse energy and recorded in a data buffer. At the end of the experiment, the data were summed and the average and standard deviation were calculated. In this configuration, a 2-mm spectrometer exit slit width translated into a total intensity measured over 3.2-nm spectral width. The spectrometer was driven such that the intensity was measured at 1.0-nm intervals. Intensity measurements were thus overlapping. Each Raman spectrum was measured with 20–25 data points.

Because of the high-number densities, measurements in the combustion chamber were possible with the use of an intensified linear array instead of a PMT. The intensifier used was red enhanced. The array consisted of 700 active pixels of 25 μm width, so that a spectral area of 28 nm was observed. The intensifier was gated to improve the SNR. The background-corrected spectra were stored in raw format and later corrected for laser pulse energy. In this configuration, some of the collected light was lost as a result of overfilling the spectrometer $f\#$ and because the inlet slit size of the spectrometer (700 μm) was set smaller than the fiber image. This was done to improve spectral resolution and reduce stray light, without a significant loss of signal.

To investigate possible spectral interference, spontaneous emission of the combustion was observed over the visual part of the spectrum with the collection system described in the previous section without the collection lens. With this optical setup, emission from a large section of the combustion chamber was observed. The result is displayed in Fig. 6. The spectrum shown was obtained with a 15-s exposure time. Some of the spectral features, relating to H_2/O_2 flame emission, are identified in Fig. 6, with the wavelength and the originating species noted. The calculated locations of the Stokes Raman spectra of oxygen, water, and hydrogen (~660, ~765, and 794 nm, respectively) are indicated with dashed lines.

During the species and temperature measurement, the Raman spectra for oxygen and water were obtained using a gated detector approach, the detector was only exposed for the duration of the laser pulse (~2.5 μs). For each experiment 140 exposures were added on the detector, giving a total exposure time of 0.4 ms during a 15-s test. This exposure length was small in comparison to the overall exposure time of the background spectrum that was shown in Fig 6. The contribution of the background emission to the Raman spectra at these locations was therefore negligible.

A single-shot spectrum provides an instantaneous picture of the molecular distribution over the rotational–vibrational energy states, which is a complex function of temperature. During a single-shot, the temperature can be assumed to be constant. Between laser pulses, however, the temperature fluctuations can be large, and consequently the shot-to-shot spectra can vary significantly in distribution. For the current measurements, single-shot data could not be obtained as the result of the weakness of the signal. Data were obtained by array accumulation of the signal scattered by all pulses during a test. A typical spectrum was an accumulated average of 140 exposures. Because the accumulated spectrum is a sum of individual spectra, the temperature extracted from a simple accumulation of distributions with widely varying temperatures does not equal the temperature that would have been obtained if the temperature at each pulse was obtained and averaged. A simulation showed that at temperatures of 2500 $\pm$ 500 K, the difference between the Raman-measured average temperature and the statistical average temperature could be as high as 3%.

Measurements

Two-Dimensional Diagnostics Thruster

Measurements were taken in the vertical plane of symmetry of the two-dimensional thruster, in a single vertical traverse at the injector exit. The distance was nondimensionalized with respect to half the injector exit height, with the origin at the centerline and unity at the injector sleeve inner wall. Data obtained were temperature, oxygen number densities, and water number densities.

The temperatures were extracted from the vibrational oxygen Raman spectra by curve fitting a model function to the measured spectrum as described in the previous section. Figure 7 displays the measured temperatures as a function of the location in the injector exit plane. Figure 7 shows that the measured data are not quite symmetric around the plane of symmetry. The nonsymmetry could be caused by statistical and measurement error, or by a nonsymmetric flow with respect to the plane of symmetry.

The lowest temperature, 1766 K, was measured at the centerline. The maximum measured temperature of 2812 K occurred at a nondimensional location of 0.6. Assuming full combustion within the injector, with equilibrium composition at the injector exit, these two temperatures correspond with local O/F ratios of 65 and 18, respectively. With an injector O/F ratio of 13.3, a large portion of the hydrogen fuel in the in-

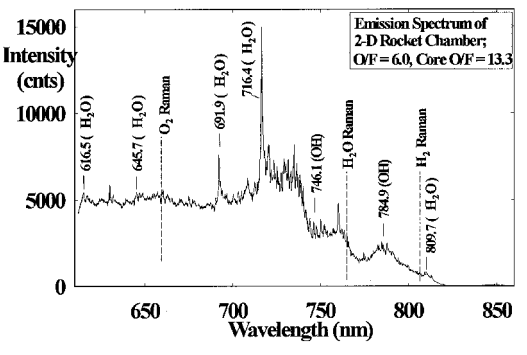

Fig. 6 Visible emission spectrum of two-dimensional diagnostics rocket.

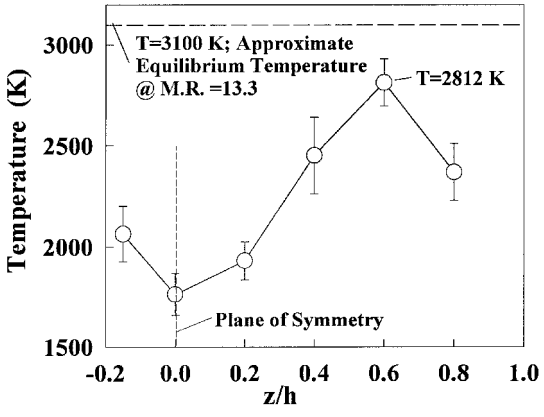

Fig. 7 Measured fuel–film sleeve exit temperature profile.

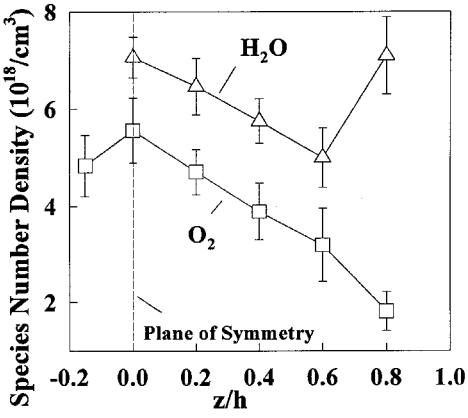

Fig. 8 Measured fuel–film sleeve exit oxygen and water number density profiles.

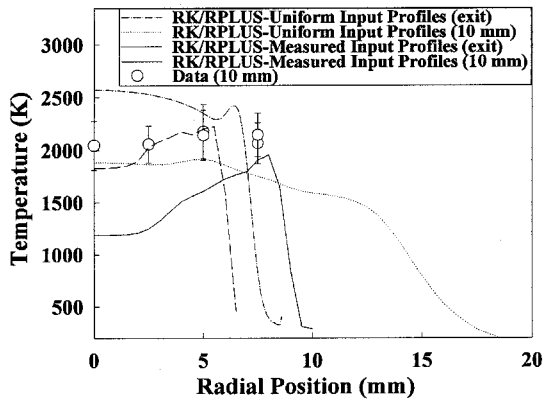

Fig. 9 Predicted and measured low-area-ratio-nozzle rocket exit temperatures.

jector is not accounted for. An explanation of this discrepancy can be rationalized from the type of injection. Hydrogen is injected radially through 12 ports into the axial oxygen core flow at a location, where the oxygen bulk velocity is approximately 240 m/s. Three-dimensional CFD simulation of the problem[23] shows that the oxygen momentum causes the hydrogen to streak downstream, without having completely mixed and reacted at the measurement location. Changing the location of the hydrogen ports (by rotation of the hydrogen injector platelet over 15 deg within its plane) could verify this, but was not feasible with the current hardware.

The temperature maximum at a nondimensional radius of 0.6 can be explained from the same scenario. The injected hydrogen jets separate from the wall and are surrounded by oxygen. Three-dimensional CFD computations[23] show that horseshoe vortices, created in the oxygen, envelope the hydrogen jet. At the jet interface, reaction takes place and the temperature will reach a maximum. At the wall, however, noncombusted oxygen will dominate, leading to a lower temperature than equilibrium chemistry with fully mixed propellants would predict. The same CFD computations show that products emanating from the reacting jet interface, and transported by means of the horseshoe vortices will penetrate toward the wall and raise the oxygen temperature.

This scenario is corroborated by the species concentration measurement. Measured oxygen and water species concentrations are shown in Fig. 8 as a function of the nondimensional injector sleeve height. As opposed to the temperature profile, the oxygen profile shows an almost symmetrical behavior. Water species measurements were only obtained above the plane of symmetry, so that no symmetry comparison could be made. The drop in both water and oxygen number densities with increasing height can be explained by the reduction in density as the result of the increasing temperature. The species could not be reported as mole fraction because no hydrogen and hydroxyl (OH) concentrations were measured. Therefore, no clear image of the combustion process could be obtained. After reaching a minimum at the location of the highest temperature, the water concentration increases again at greater height, whereas the oxygen concentration continues to decrease. This supports the previously described scenario, where water from the reacting jet interface is transported by means of the oxygen-rich horseshoe vortices toward the wall.

Hydrogen was not detected at any of the measured locations. An effort to measure hydrogen in the fuel–film layer was unsuccessful. This was partly because of the wall presence, which caused saturation of the array as the result of wall scattering.

Because of the lack of complete species measurements, no mass balance could be obtained to verify the accuracy of the results. Measurements, however, showed that the conventional approach of modeling the thruster flow by means of assuming uniform injector exit boundary conditions caused the prediction to be in significant error. A more accurate determination of boundary conditions is needed to make CFD predictions acceptable.

Low-Area-Ratio Nozzle

The effect of the inlet boundary conditions on the flowfield calculations was investigated by comparing two sets of results from RPLUS code flowfield predictions with measurements obtained 10 mm downstream of the low-area-ratio nozzle. The two sets of boundary conditions used to obtain the RPLUS predictions were 1) a uniform injector exit profile in temperature, species, and velocity with fully mixed and reacted propellants, and 2) measured temperature and species profiles at the injector exit and a uniform velocity profile. The species profiles were complemented by assuming equilibrium chemistry at each location and calculating hydroxyl and hydrogen concentrations from the measured oxygen, water, and temperature profiles.

Only temperature and oxygen number densities were obtained 10 mm downstream of the nozzle exit plane. The measured water spectra were too weak to extract reliable data. The comparison of the resulting predicted temperature profiles with the measured data at this location is shown in Fig 9. The temperature calculated at the exit plane is added to Fig. 9 to visualize how the flowfield expands, according to the RPLUS code, from the exit plane to the 10 mm downstream plane.

No measurements were obtained at radial distances further than 7.5 mm because of the absence of oxygen in those areas. The temperature measured at the centerline was approximately 2050 K, significantly lower than would be expected from a fully combusted mixture with an O/F ratio of 5.13. The temperature increased gradually in the radial direction and reached a weak maximum of 2170 K at 5 mm radial distance after which it decreased. The measured profile was underpredicted by the RPLUS code using the uniform inlet conditions by 200–300 K. The underprediction while using the measured injector profiles was severe, between 850 K at the centerline and 1150 K at 7.5 mm radial distance. This severe underprediction had two underlying causes. The measured profiles indicated an incompletely mixed and reacted injector exit flow. The criteria inherent in the RPLUS code caused the combustor flow to be treated as fully laminar, leading to a very low mixing percentage. As a result, a large part of the propellants were not consumed in the code calculations, leading to the low-temperature prediction.

The measured oxygen number densities 10 mm downstream the exit plane are shown in Fig. 10 as a function of the radial location. The predicted number densities at the exit plane are shown as a comparison. The prediction using the uniform inlet conditions underpredicts from the centerline to a radial distance of approximately 6 mm, after which the prediction overestimates the concentration. For uniform inlet conditions, more oxygen would be consumed in the injector than measurements

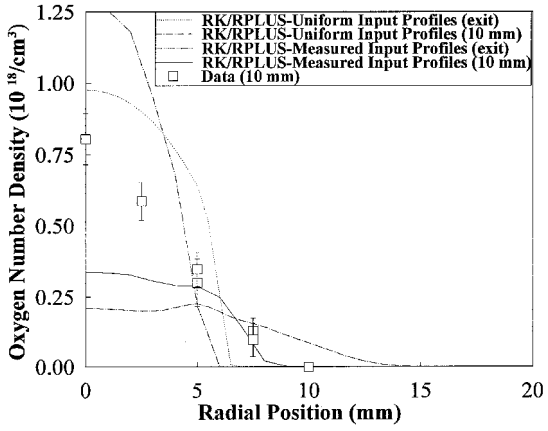

Fig. 10 Predicted and measured low-area-ratio-nozzle rocket exit oxygen number densities.

show, the effect of which propagates downstream, causing underprediction in the core. The overprediction of oxygen number densities at the outer region of the plume calls into question the fully laminar assumption of the code.

The prediction using the measured profiles as input conditions shows a better comparison from around 5 mm radial distance outward. In the core, the prediction still strongly underpredicts, even though the comparison is better than for the uniform inlet conditions. This underprediction is remarkable, especially in view of the low-temperature measurement. A lower temperature seems to indicate less oxygen consumption. Instead, the analytical results show a higher oxygen consumption than measured. The RPLUS code was adapted to include unsteadiness, but this change did not noticeably change the local predictions.

Because the code-imposed laminar nature of the flow precluded sufficient mixing in the combustor, it was found that a three-dimensional model was needed to accurately predict the large-scale mixing between the hydrogen and oxygen in the injector and combustion chamber. To fully utilize this change, it was not sufficient to assume injector exit conditions and to model downstream from there. It was necessary to include the full injector in the computations. Twelve radial hydrogen injector ports were present, thus the injector was split in 12 pie slices of 30 deg each, with the interface between the slices governed by the condition that all properties were mirrored with respect to the interface. Thus, only a single pie slice had to be computed. Preliminary results show that the flow is strongly three dimensional, and that an axisymmetric code will not do justice to the predictions. The injector flow strongly influences the mixing and reactions inside the combustion chamber. Further three-dimensional modeling is needed to better predict the performance parameters for these small thrusters from Navier–Stokes-based codes.

In an investigation to study the effect of a change in injector exit velocity profile, the measured species and temperature profiles were complemented with a wake profile instead of the uniform velocity profile. The wake profile was generated by interpolating experimental results, obtained in a reacting backward-facing step flow.[24] The nondimensional radial and axial velocity profiles were adapted for the current injector flow by enforcing mass and species conservation. The maximum radial velocity was less than 10% of the maximum axial velocity, resulting in a very small increase in mixing above the mixing predicted for the uniform velocity profiles. As a result, the final species, temperature, and velocity profiles did not change significantly.

Conclusions

To investigate the accuracy of predicting global performance parameters of small onboard thrusters by means of axisymmetric Navier–Stokes-based codes, a study was done to compare locally measured flow variables with predicted values. The Navier–Stokes code used was RPLUS.

Raman-scattering measurements were made at the exit of the injector sleeve and at 10 mm downstream of a low-area-ratio nozzle. Vibrational temperatures, oxygen, and water number densities were measured at several radial positions. These measurements showed that the conventional uniform temperature and species profiles, used in predicting global performance parameters for this specific thruster were far from correct. Hydrogen did not penetrate the recirculation zone behind the spark plug, and therefore did not thoroughly mix with the oxygen, leading to incomplete combustion. The core of the injector flow showed a relatively low-temperature, oxygen-rich mixture. The maximum temperature was found at a nondimensional radial location of 0.6, indicating that a reaction zone was present.

Using the measured temperature and species injector profile as input condition to the RPLUS code did not improve global performance parameters. The computed global results were also insensitive to a change in assumed injector exit velocity profile. Laminar conditions in the combustor, as predicted by the code, did not allow mixing sufficient to increase predicted performance. A turbulent injector exit profile could lead to enhanced mixing of the combustion chamber core with the fuel–film at the wall.

Predicted temperature and oxygen number density profiles 10 mm downstream of a low-area-ratio-nozzle combustor did not compare well with measured values for either set of input conditions, the uniform or the measured profiles. Both the temperatures and oxygen number densities were underpredicted. The underprediction was worse for the measured profile input case as the result of the incomplete injector combustion detected with these measurements, which caused a lower combustion efficiency and subsequently a lower performance.

The laminar nature of the flow as predicted by the axisymmetric RPLUS code precluded an improved prediction of both global performance and local flowfield data. It was concluded that to better predict these small thruster flows, a three-dimensional modeling of the thruster with the inclusion of the injector was needed.

References

[1]Reed, B. D., "Long Life Testing of Oxide-Coated Iridium/Rhenium Rockets," AIAA Paper 95-2401, July 1995.

[2]Schoenman, L., "4000°F for Low Thrust Rocket Engines," AIAA Paper 93-2406, June 1993.

[3]Schneider, S. J., "Low Thrust Chemical Rocket Technology," NASA TM-105927, International Astronautical Federation, Paper 92-0669, Sept. 1992.

[4]Arrington, L. A., and Reed, B. D., "Performance Comparison of Axisymmetric and Three-Dimensional Hydrogen Film Coolant Injection in a 110-N Hydrogen/Oxygen Rocket," AIAA Paper 92-3390, July 1992.

[5]Jankovsky, R. S., "HAN-Based Monopropellant Assessment for Spacecraft," AIAA Paper 96-2863, July 1996.

[6]Richter, G. P., and Price, H. G., "Proven, Long-Life Hydrogen/Oxygen Thrust Chambers for Space Station Propulsion," JANNAF Propulsion Meeting, New Orleans, LA, Aug. 1986; also NASA TM-88822.

[7]Weiss, J. M., "Analysis of Reacting Flowfields in Low-Thrust Rocket Engines and Plumes," Ph.D. Dissertation, Pennsylvania State Univ., University Park, PA, Dec. 1992.

[8]Zupanc, F. J., and Weiss, J. M., "Rocket Plume Flow Field Characterization Using Laser Rayleigh Scattering," AIAA Paper 92-3351, July 1992.

[9]Zupanc, F. J., "Pulsed Laser Rayleigh Scattering Diagnostic for Hydrogen/Oxygen Rocket Exit Plane Flow Field Velocimetry," AIAA Paper 93-0805, Jan. 1993.

[10]De Groot, W. A., and Weiss, J. M., "Species and Temperature Measurement in H_2/O_2 Rocket Flow Fields by Means of Raman Scattering Diagnostics," AIAA Paper 92-3353, July 1992.

[11]Weiss, J. M., and Merkle, C. L., "Numerical Investigation of Re-

acting Flowfields in Low-Thrust Rocket Engine Combustors," AIAA Paper 91-2080, June 1991.

[12]Weiss, J. M., Daines, R. L., and Merkle, C. L., "Computation of Reacting Flowfields in Low-Thrust Rocket Engines," AIAA Paper 91-3557, Sept. 1991.

[13]Anon., *JANNAF Rocket Engine Performance Prediction and Evaluation Manual*, Chemical Propulsion Information Agency, Publication 246, April 1975.

[14]Robinson, P. J., "Space Station Auxiliary Thrust Chamber Technology," GenCorp Aerojet, NASA CR-185296, Sacramento, CA, July 1990.

[15]James, T. C., and Klemperer, W., "Line Intensities in the Raman Effect of $^1\Sigma$ Diatomic Molecules," *Journal of Chemical Physics*, Vol. 31, No. 1, 1959, pp. 130–134.

[16]Shirley, J. A., "Investigation of the Feasibility of Temperature Profiling Optical Diagnostics in the SSME Pre-Burner," Final Tech. Rept., NAS8-34774, June 1983.

[17]Mizushima, M., *The Theory of Rotating Diatomic Molecules*, Wiley, New York, 1975.

[18]Murphy, W. F., Holzer, W., and Bernstein, H. J., "Gas Phase Raman Intensities: A Review of 'Pre-Laser' Data," *Applied Spectroscopy*, Vol. 23, No. 3, 1969, pp. 211–218.

[19]Asawaroengchai, C., and Rosenblatt, G. M., "Rotational Raman Intensities and the Measured Change with Internuclear Distance of the Polarizability Anisotropy of H_2, D_2, N_2, O_2, and CO," *Journal of Chemical Physics*, Vol. 72, No. 4, 1980, pp. 2664–2669.

[20]Jones, R. A., De Groot, W. A., Myrabo, L. N., and Nagamatsu, H. T., "Experimental Investigation of Vibrational Nonequilibrium in H_2O_2 Rocket Engines," AIAA Paper 96-0228, Jan. 1996.

[21]Jones, R. A., De Groot, W. A., Myrabo, L. N., and Nagamatsu, H. T., "Oxygen Temperature and Concentration Measurements in H_2O_2 Rocket Engines," AIAA Paper 96-0439, Jan. 1996.

[22]Eckbreth, A. C., Bonczyk, P. A., and Verdieck, J. F., "Review of Laser Raman and Fluorescence Techniques for Practical Combustion Diagnostics," Rept. EPA-600/7-77-066, June 1977.

[23]Tsuei, H. H., and Merkle, C., "Mixing and Reaction in a Combustor with Transverse Jet Injection," AIAA Paper 95-2171, June 1995.

[24]Wu, M. Z., Walterick, R. E., De Groot, W. A., Jagoda, J. I., and Strahle, W. C., "Turbulent Diffusion Flame Properties Behind a Backward-Facing Step," *Journal of Propulsion and Power*, Vol. 8, No. 5, 1992, pp. 948–953.